Chemical Science

ROYAL SOCIETY OF CHEMISTRY

EDGE ARTICLE

View Article Online
View Journal | View Issue

Cite this: *Chem. Sci.*, 2024, **15**, 13313

All publication charges for this article have been paid for by the Royal Society of Chemistry

Received 14th February 2024
Accepted 9th July 2024

DOI: 10.1039/d4sc01029a

rsc.li/chemical-science

A physics-aware neural network for protein–ligand interactions with quantum chemical accuracy†

Zachary L. Glick, [a] Derek P. Metcalf, [a] Caroline S. Glick, [a] Steven A. Spronk, [b] Alexios Koutsoukas, [b] Daniel L. Cheney [b] and C. David Sherrill *[a]

Quantifying intermolecular interactions with quantum chemistry (QC) is useful for many chemical problems, including understanding the nature of protein–ligand interactions. Unfortunately, QC computations on protein–ligand systems are too computationally expensive for most use cases. The flourishing field of machine-learned (ML) potentials is a promising solution, but it is limited by an inability to easily capture long range, non-local interactions. In this work we develop an atomic-pairwise neural network (AP-Net) specialized for modeling intermolecular interactions. This model benefits from a number of physical constraints, including a two-component equivariant message passing neural network architecture that predicts interaction energies *via* an intermediate prediction of monomer electron densities. The AP-Net model is trained on a comprehensive dataset composed of paired ligand and protein fragments. This model accurately predicts QC-quality interaction energies of protein–ligand systems at a computational cost reduced by orders of magnitude. Applications of the AP-Net model to molecular crystal structure prediction are explored, as well as limitations in modeling highly polarizable systems.

1 Introduction

Non-covalent interactions (NCIs) play a key role in the chemical sciences. Although they are weaker than covalent bonds, the presence (or absence) of NCIs can have profound effects on chemical and biomolecular systems. For example, NCIs drive DNA intercalation—the insertion of a molecule between consecutive DNA base pairs—which is the mechanism of action in anti-cancer drugs such as doxorubicin.[1,2] Not only can an understanding of NCIs provide mechanistic insights into intercalation and other small molecule binding modes, careful consideration of NCIs allows one to control the selectivity of reaction catalysts,[3] enhance electrochemical reaction kinetics,[4] or optimize the properties of nanostructures.[5]

NCIs play a particularly important role in small molecule drug design. The efficacy of a drug depends in part on the presence of strong interactions with the target protein. Often, preliminary drug design efforts produce a promising but sub-optimal "lead" compound. This lead compound is then iteratively revised in an attempt to enhance desired properties. Maximizing favorable intermolecular contacts is a critical aspect of the lead optimization process, and can be aided by *in silico* models of NCIs.

The strength of a protein–ligand interaction can be rigorously quantified by using the tools of quantum chemistry to compute an interaction energy. Quantum chemistry methods, which seek to solve the many-body Schrödinger equation, are subject to a well-established trade-off between computational cost and accuracy. Highly accurate interaction energies can be obtained from wavefunction-based methods such as coupled cluster (CC) theory, but such calculations are often too expensive for all but the smallest systems. Less expensive methods like density functional theory (DFT) yield slightly less robust interaction energies. Simple, transferable force fields like GAFF are orders of magnitude faster than any quantum chemistry method, but force field interaction energies are only semi-quantitatively accurate.

One quantum chemistry method of particular interest for studying protein–ligand interactions is symmetry-adapted perturbation theory (SAPT), which yields not only an interaction energy, but also its physically meaningful components: electrostatics, exchange-repulsion, induction/polarization, and London dispersion.[6–8] These components provide additional insight to help understand non-covalent interactions.[9] The fragment-based partitioning of SAPT[10] was used to understand substituent effects in protein–ligand interactions in factor Xa inhibitors.[11] However, models of the protein including only nearby residues (~200 atoms) still required many hours of CPU time for the SAPT computations.

[a]*School of Chemistry and Biochemistry, School of Computational Science and Engineering, Georgia Institute of Technology, Atlanta, Georgia, 30332-0400, USA. E-mail: sherrill@gatech.edu*

[b]*Molecular Structure and Design, Bristol Myers Squibb Company, P.O. Box 5400, Princeton, New Jersey 08543, USA*

† Electronic supplementary information (ESI) available: Table S1 describing the SAPT0 decomposition of the $\Delta\Delta E$ results. Fig. S1 showing one-dimensional slices of Fig. 6. SAPT0 interaction energies and Cartesian coordinates of the 13 216 validation set dimers and nine protein–ligand matched pairs. See DOI: https://doi.org/10.1039/d4sc01029a

Recently, advances in machine learning (ML) have led to the re-evaluation of this classic cost-accuracy trade-off. Models like neural networks (NNs) are capable of expressing arbitrarily complicated non-linear functions such as molecular potential energy surfaces.[12–16] Large datasets of quantum chemical computations[17–20] make it possible to parameterize general atomistic NN potentials to quantum chemical accuracy,[21–23] and these potentials can be evaluated at near force field computational cost. NN potentials can be used to improve the accuracy of costly alchemical free energy predictions[24] or to perform reactive molecular dynamics simulations.[25]

The emergence of NN potentials has also benefited from a number of architectural developments. The "message passing" NN (MPNN) framework is tailored to the graph-like structure of molecular geometries.[26] Directional MPNNs additionally account for the relative orientation between neighboring atoms in a molecule. The most data-efficient architectures achieve this by employing locally equivariant representations of atoms in molecules.[27–33] In these equivariant models, atomic environments are represented as tensorial quantities which rotate with the local coordinate frame.

The locality of atomic environments used in NN potentials allows these models to easily describe local interactions, which include distortions of bonds, angles, and dihedrals, as well as short-range non-covalent interactions. Unfortunately, a consequence of this locality is that NN potentials are either indirectly or explicitly unable to model the long-range interactions that are essential to protein–ligand interactions.[34] The lack of these long-range effects has been demonstrated to affect the quality of simulated properties of bulk water and small peptides,[35] and many ML methods have been developed to capture these long-range interactions.[36–38] In a recent work, we proposed an atomic-pairwise NN framework for modeling NCIs, which we called AP-Net.[34] Extending this basic proof-of-concept, we now develop a robust, chemically accurate AP-Net model for quantifying arbitrary protein–ligand interactions. This is accomplished by constraining the AP-Net architecture to respect the known physics of intermolecular interactions.

2 Results

2.1 A physics-aware intermolecular architecture

In this work, we develop a physics-aware neural network architecture specialized for modeling intermolecular interactions. This architecture adheres to four physical principles:

1. Intermolecular interactions are fundamentally a function of molecular properties, some of which, such as the electron density, can be partitioned into atomic properties.

2. For the most part, intermolecular interactions are atomic-pairwise additive.

3. Intermolecular interactions are decomposable into different types of interactions (electrostatics, exchange-repulsion, induction/polarization, and dispersion).

4. In the dissociative limit, intermolecular interactions obey simple functional forms of molecular and atomic properties and smoothly decay to zero.

In reference to the second principle, this physics-aware architecture is designated AP-Net, short for atomic-pairwise neural network. The AP-Net name was first used in a previous proof-of-concept study that differs significantly from the current work in applicability and complexity.[34] The previous AP-Net architecture shares the general paradigm of predicting interaction energies in an atomic-pairwise framework, but the previous model was limited by simple, ad hoc atomic feature vectors whereas the model described in this work featurizes atom pairs with an equivariant MPNN (Section 2.1.2). The current AP-Net model is additionally differentiated by the inclusion of an electrostatic force field, a related atomic property module (Section 2.1.1), and a much larger, more diverse training set (Section 2.2).

A schematic of the current AP-Net architecture is provided in Fig. 1. AP-Net enforces the four physical principles above *via* a pair of independently trained NNs, which are respectively referred to as the atomic property module and the interaction energy module. These two NNs are used to predict protein–ligand interaction energies through an intermediate prediction of the electron density of both molecules *via* an atom-centered multipole expansion. This physically motivated functional form yields accurate, generalizable interaction energy predictions for protein–ligand systems.

2.1.1 Atomic property module. The atomic property module (Fig. 1A) is trained to predict properties of an atom within a molecule, in accordance with the first principle. Specifically, this network predicts an atomic decomposition of the electron density in the form of an atom-centered multipole expansion through second order. The atomic property module is related to our previous Cartesian MPNN (CMPNN), which was also used to predict atomic multipoles.[39] Unlike the original CMPNN model, in which predicted atomic multipoles were approximately rotationally equivariant, the atomic property module enforces rigorous rotational equivariance *via* the directional hidden state scheme of ref. 27. In this scheme, the hidden state vectors have an additional Cartesian dimension, along which equivariance is preserved by a carefully designed message and update function. The atomic property module also conserves the total molecular charge, allowing the model to handle neutral molecules and ions alike.[40]

2.1.2 Interaction energy module. The second neural network constituting AP-Net, the interaction energy module (Fig. 1B), is an equivariant graph neural network trained to predict the interaction energy of a molecular dimer. This interaction energy is predicted as a sum of atom-pair contributions. Rather than directly predict the total interaction energy, this module predicts the symmetry-adapted perturbation theory (SAPT) decomposition of the interaction energy into its components of electrostatics, exchange, induction, and dispersion. The interaction energy module architecture is described in detail in Section 3.1.2.

Most notably, instead of operating on only the dimer geometry, the interaction energy module operates on the output of the atomic property module—atom-centered multipoles through second order and hidden-state vectors encoding atomic environments—evaluated separately for each monomer.

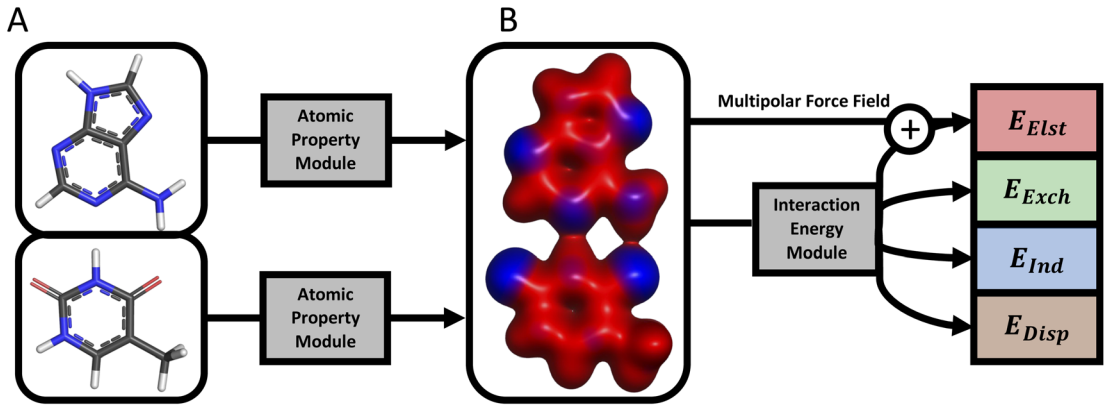

Fig. 1 An overview of the AP-Net architecture where (A) is the atomic property module and (B) is the interaction energy module. AP-Net predicts the four physically meaningful components of a protein–ligand interaction: electrostatics (E_{elst}), exchange (E_{exch}), induction/polarization (E_{ind}), and London dispersion (E_{disp}).

The output of the atomic property module is used by the interaction energy module in two ways. First, the learned representation of each atomic environment from the atomic property module is incorporated into the corresponding atomic environment in the interaction energy module. This shared representation allows the interaction energy module to indirectly utilize the monomer data used to train the atomic property module. Second, the predicted atomic multipoles of the atomic property module are used to evaluate a multipolar electrostatic energy. The interaction energy module is then trained to predict the interaction energy as a correction on top of the multipolar electrostatic energy. Because the multipolar electrostatic energy captures the leading long-range behavior of intermolecular interactions, the interaction energy module is effectively limited to predicting a much more local, medium- and short-range quantity.

This strategy of combining two different methods is similar to the correction-based concept of Δ-learning, in which one reformulates a regression task as a small predicted correction on top of a computationally affordable baseline result.[41] However, unlike conventional Δ-learning use cases in quantum chemistry, the baseline model, multipole electrostatics *via* predicted multipoles, is as computationally affordable as the machine learning correction.

2.2 Systematically-generated protein–ligand interactions

The Splinter dataset[42] is a collection of approximately 1.7 million systematically generated protein–ligand fragment dimers and interaction energies computed using many-body SAPT based on a Hartree–Fock (HF) representation of monomers (*i.e.* SAPT0). These and all other SAPT computations carried out in this work are performed in an aug-cc-pV(D+d)Z basis set (abbreviated aDZ), which yields good error cancellation.[43] The construction of this dataset is illustrated in Fig. 2A. The Splinter dimers are not only chemically diverse, they also were intentionally generated in

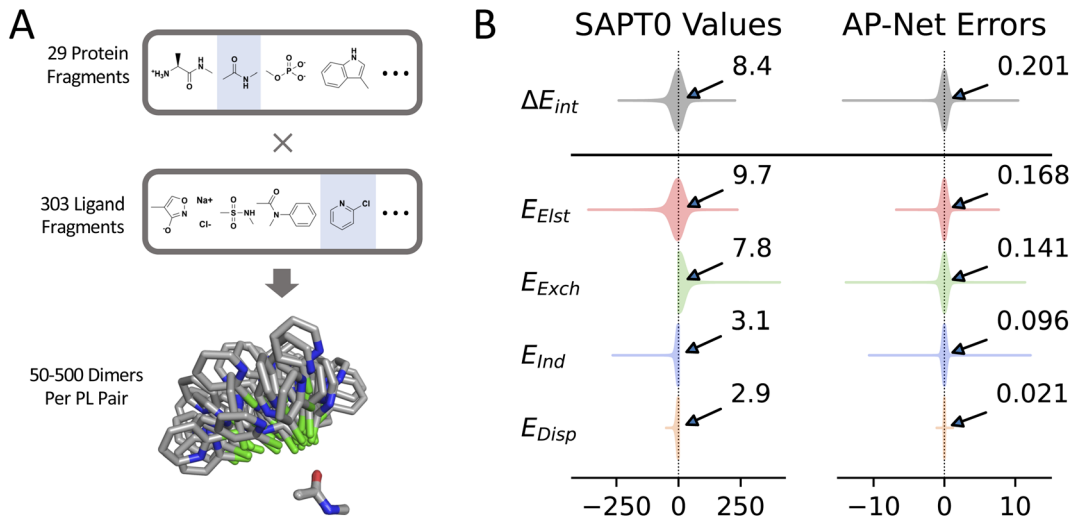

Fig. 2 (A) Depiction of the Splinter dimer dataset. This dataset was constructed by exhaustively pairing small protein and ligand fragments. Between 50 and 500 dimer configurations were generated for each pair of fragments. (B) Distribution of interaction energies (left) and AP-Net errors with respect to interaction energies (right) over 150 000 validation dimers of the Splinter dataset, in kcal mol^{-1}. The respective mean absolute interaction energies and mean absolute errors of the two sets of distributions are labeled.

variety of repulsive, optimized, and dissociated configurations. Consequently, the interaction energies associated with the Splinter dimers span a range of over 500 kcal mol^{-1}.

A large fraction of the Splinter dataset was used to train the interaction energy module of the AP-Net model. The performance of AP-Net on 150K held-out validation dimers, which were not used to fit the model, is shown in Fig. 2B. AP-Net predicts the SAPT interaction energies with a mean absolute error (MAE) of only 0.20 kcal mol^{-1} and a maximum error of less than 15 kcal mol^{-1}. The interaction energy of over 97% of the validation dimers is predicted within 1 kcal mol^{-1}, a metric commonly referred to as chemical accuracy.[44] The individual SAPT components of the interaction energy are predicted with even greater accuracy than the total interaction energy. As observed in previous efforts to predict the SAPT decomposition with ML models, errors in electrostatics and exchange are largest, followed by induction, and then dispersion.[34,45] Dispersion is predicted particularly accurately, with a MAE of only 0.02 kcal mol^{-1}. It should be noted that the error in this prediction is much smaller than errors inherent in the SAPT0 approximation or even the choice of finite basis set.

2.3 Crystallographic protein–ligand interactions

The ultimate goal of the AP-Net intermolecular potential is to accurately predict interaction energies of realistic models of protein–ligand systems. Therefore, it would not be sufficient to only evaluate the model on dimers sampled from Splinter, which are procedurally generated and come from the same chemical space as the training data. For this reason, we developed a more diverse, realistic dataset of dimers, referred to as SAPT-PDB-13K. The 13 216 dimers in SAPT-PDB-13K consist of an entire ligand interacting with one or two capped amino acids. The protein and ligand geometries are taken from crystallographic Protein Data Bank (PDB) entries, making them meaningful and practical test cases. An illustrative dimer from the SAPT-PDB-13K dataset is shown in Fig. 3.

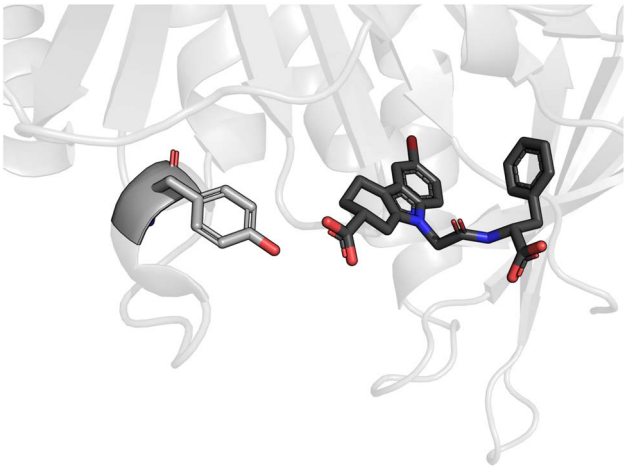

Fig. 3 An example dimer from the SAPT-PDB-13K dataset. A small molecule inhibitor interacts with the nearest amino acid, a tyrosine, of an *Escherichia coli* sliding clamp protein. This dimer was extracted from PDB entry 4PNU.

The diversity of the SAPT-PDB-13K dataset makes it a useful test of AP-Net's generalization ability. Compared to the Splinter dataset, SAPT-PDB-13K contains different, larger ligands that span more charge states. Regardless, Fig. 4 shows that AP-Net still accurately predicts the SAPT0 interaction energy decomposition with a MAE of 0.74 kcal mol^{-1}. In many ways, the prediction errors on the SAPT-PDB-13K dimers resemble the prediction errors on the held-out Splinter dimers. One notable difference is in the prediction of the SAPT induction term. Interestingly, the induction MAE is larger relative to the other three SAPT components. It is also apparent from Fig. 4 that the predicted induction energies have a slight positive bias for dimers with large, negative induction energies. This observation is in line with the fact that induction is an inherently many-body phenomenon, in contrast to the atomic-pairwise additivity of AP-Net.[46] The many-body nature of induction—which can be thought of as mutual polarization between three or more atoms combined with charge transfer—becomes apparent in a few SAPT-PDB-13K dimers that contain strongly interacting di- and tri-anions.

2.4 Relative interaction energies

AP-Net's performance on the Splinter and SAPT-PDB-13K datasets demonstrates the model's ability to accurately predict interaction energies (ΔE_{int}) of protein–ligand systems. A derived quantity of interest is the relative interaction energy ($\Delta\Delta E_{\text{int}}$), defined as the difference in interaction energies between two related dimers, such as those that differ by a change in a single functional group. An example experiment is illustrated in Fig. 5. Such single-point alchemical computations may be used to guide the drug design process.

The results of nine $\Delta\Delta E_{\text{int}}$ experiments are listed in Table 1, and a breakdown by SAPT component is included in the ESI.† In each experiment, the $\Delta\Delta E_{\text{int}}$ of two related protein–ligand dimers is calculated using both SAPT and AP-Net. Each pair of dimers is constructed from an initial protein–ligand complex, taking a portion of the ligand and its surrounding protein environment.[47] The second dimer of each pair is characterized by a change in a ligand functional group. In seven of the nine pairs, a chlorine is replaced with a methyl group, and in 2O7N, a cyano group is replaced with a bromine. The ligands of the 2Y5G/2Y5H matched pair differ by a heterocycle rotation rather than an atomic substitution. In all nine computational experiments, the sign of the AP-Net $\Delta\Delta E_{\text{int}}$ matches the sign of the SAPT-computed $\Delta\Delta E_{\text{int}}$, meaning the AP-Net interaction energies are accurate enough to predict whether each functional group substitution stabilized or destabilized the protein–ligand interaction. SAPT0 computations on some of these complexes (~200 atoms) required as much as 1.5 days or more, running on 12 cores, while the AP-Net computations ran in a few seconds each. This makes *in silico* ligand design experiments of this type (with quantum-mechanical accuracy) now feasible for routine and easy use.

2.5 Transfer learning to gold standard quantum chemistry

The SAPT0/aDZ level of theory used in the Splinter dataset has been extensively benchmarked and strikes a good balance between computational cost and accuracy.[43] A more accurate

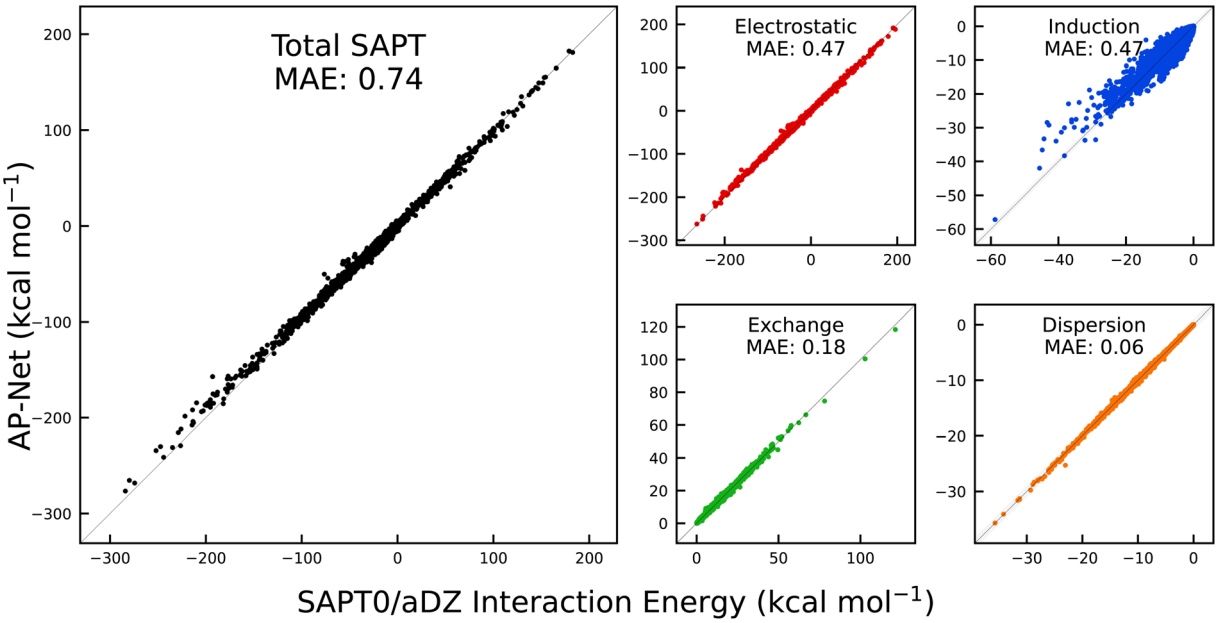

Fig. 4 Correlation between AP-Net predicted interaction energies and computed SAPT0/aDZ interaction energies on the 13 216 dimers in the SAPT-PDB-13K dataset.

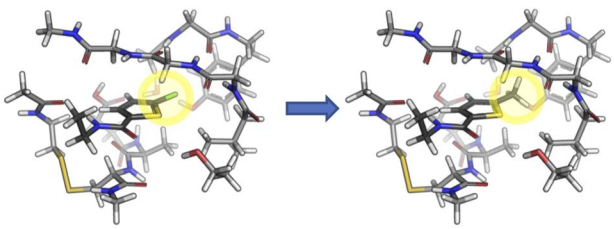

Fig. 5 Example of an alchemical $\Delta\Delta E_{int}$ experiment. The chlorine group of the P1 substructure of the Factor Xa inhibitor, BAY 59-7939, is mutated to a methyl. The structure is extracted from PDB entry 2W26.

Table 1 Difference in interaction energies (kcal mol^{-1}) for alchemical substitutions in nine protein–ligand complexes. The PDB entry of the crystallographic structures from which each dimer pair was derived is given

PDB entry	SAPT0 $\Delta\Delta E_{int}$	AP-Net $\Delta\Delta E_{int}$
2CJI	−2.07	−1.67
2O7N	+4.16	+4.26
2PR3	−1.03	−1.42
2UZT	+0.17	+0.91
2W26	−2.00	−1.00
2Y5(G/H)	−3.47	−3.65
3ENS	−4.95	−2.94
4YFF	+0.86	+0.38
4YHT	−2.23	−2.97

level of theory is coupled cluster with singles, doubles, and perturbative triples [CCSD(T)][48] in the complete basis set (CBS) limit. CCSD(T)/CBS is often referred to as the "gold standard" in quantum chemistry because of its reliability. Ideally, the AP-Net model would be trained on CCSD(T)/CBS interaction energies for the Splinter dimers, but the steep $\mathcal{O}(N^7)$ scaling of this method makes obtaining many such high-quality interaction energies prohibitively expensive. An appealing solution from the field of machine learning is the process of transfer learning, in which one leverages data associated with one task (predicting SAPT0/aDZ interaction energies) to improve performance at some other similar, usually data-limited task (predicting CCSD(T)/CBS interaction energies).[49] Generally, transfer learning is realized by initially training some NN model on the first large dataset, and then re-training the same model on the smaller, relevant dataset. This approach has been successfully used in the development of atomic potentials.[50]

A transfer learning experiment was performed to assess the practicality and data requirements of training a CCSD(T) quality AP-Net intermolecular potential. This experiment was performed with the DES370K dimer dataset.[20] DES370K is similar to the Splinter dataset in that it contains many small molecule dimers. Unlike Splinter, DES370K contains interaction energies computed at the CCSD(T)/CBS level of theory. Two separate "AP-Net-CC" models were trained on the DES370K dataset to predict CCSD(T)/CBS interaction energies. These models are referred to as AP-Net-CC to differentiate them from the standard AP-Net model, which is fit to the SAPT decomposition. Because AP-Net is constructed to separately predict the four SAPT interaction energy components, all AP-Net-CC models are trained so that the sum of the four predicted components matches the CCSD(T)/CBS interaction energy. Therefore, any AP-Net-CC model lacks the interpretability of an AP-Net model trained to predict the SAPT decomposition. As a baseline, the first AP-Net-CC model was constructed with randomly initialized weights in the interaction energy module. The second "pre-trained" AP-Net-CC model was constructed with interaction energy module weights taken from the original AP-Net model. Both AP-

Net-CC models used the same frozen atomic property module as the original AP-Net model.

The accuracy of the two AP-Net-CC models as a function of the amount of DES370K training data is shown in Table 2. The pre-trained AP-Net-CC model outperforms the baseline AP-Net-CC model, particularly in the low data regime. At 100 training data points, transfer learning results in a nearly four-fold error reduction (from 1.91 kcal mol^{-1} to 0.48 kcal mol^{-1}). The accuracy of a pre-trained AP-Net-CC model with only 100 training data points is similar to that of a baseline AP-Net-CC trained on a few thousand data points. Transfer learning provides diminishing returns when more CCSD(T)/CBS data is available. The pre-trained model is nearly equivalent to the baseline model when 50K training points are used. These results demonstrate that transfer learning is an economical approach for leveraging the original AP-Net model, which was trained on the SAPT decomposition of over 1.5 M dimers, to predict interaction energies at more computationally expensive levels of theory. A minimal amount of expensive, high accuracy CCSD(T)/CBS data is required to fine-tune AP-Net from SAPT to this gold standard quantum chemistry method.

2.6 Predicting interaction energy surfaces

The transfer learning approach applies not just between different levels of quantum chemical theory, but also between different regions of chemical space. In particular, one might want to repurpose the AP-Net potential, which is parameterized to model protein–ligand interactions in general, into an interaction energy model specialized for a particular dimer, which may not even be a protein–ligand system. To explore the usefulness of such a model, we examined the performance of the previously described AP-Net-CC models on the interaction energy surface of the hydrogen-bonded *N*-methylacetamide (NMA) dimer. This dimer is a model system for peptide bonding. SAPT0/aDZ and CCSD(T)/CBS interaction energies were computed along a two-dimensional scan of the intermolecular hydrogen bond length and angle of this dimer. The intermolecular O···H bond length was varied from 1.5 Å to 3.0 Å in 0.1 Å increments and the intermolecular O··· HN bond angle from −90° to +90° in 1.5° increments. Fig. 6 shows these reference interaction energy surfaces compared to predictions of the AP-Net and two AP-Net-CC models. An additional one-dimensional visualization of this surface is available in the ESI.† The computed SAPT0/aDZ and CCSD(T)/CBS surfaces differ by a small amount: the SAPT0/aDZ surface is overall lower in energy than the gold standard reference method, with a minimum energy of −8.43 kcal mol^{-1} at a hydrogen bond length of 2.0 Å. The CCSD(T)/CBS surface has a minimum energy of −7.28 kcal mol^{-1} at 2.0 Å.

The AP-Net predicted surface agrees with with the reference SAPT surface. This is expected given the quantity and diversity of data used to train the model. The baseline AP-Net-CC model trained on only 100 data points poorly predicts the CCSD(T)/CBS surface. This predicted interaction energy surface lacks both a repulsive wall and a reasonable minimum. However, using the same 100 points to repurpose the AP-Net model to the CCSD(T)/CBS theory with transfer learning results in an excellent prediction of the interaction energy surface. It's particularly notable that these 100 dimers are randomly selected from the DES370K dataset, and do not include NMA.

Table 2 Mean absolute errors (kcal mol^{-1}) of AP-Net-CC predicted CCSD(T)/CBS interaction energies from the DES370K dataset. The AP-Net-CC models are trained on varying amounts of randomly selected data from the same dataset. Baseline models, which are trained from scratch, are compared to a transfer learning scheme that starts with an AP-Net model pre-trained on SAPT0/aDZ interaction energies

Training dimers	Baseline	Pre-trained
100	1.91	0.48
200	1.64	0.47
500	1.22	0.40
1000	0.80	0.37
2000	0.56	0.33
5000	0.35	0.29
10 000	0.26	0.23
20 000	0.20	0.18
50 000	0.14	0.12

2.7 Ranking molecular crystal polymorphs

Intermolecular interactions largely govern the structure of molecular crystals and other clusters, making these systems a promising application of AP-Net outside of protein–ligand interactions. A vast majority of molecular crystals are polymorphic, meaning that they can exist in multiple stable crystalline forms, with potentially different physical properties like density, solubility, hygroscopicity, melting point, *etc.*[51] In drug development, thoroughly determining all polymorphs of a drug candidate is a necessary procedure that is routinely guided by computation. A common crystal structure prediction (CSP) task is to screen and rank the most energetically stable putative polymorphs of a target molecule.[52] Using the many body expansion (MBE), the energy of a crystal lattice can be recast as approximately a sum of many dimer interaction energies.[53] This two-body contribution to the crystal lattice energy, hereafter referred to as the crystal lattice energy, can therefore be computed with any quantum chemistry method used for interaction energies or predicted with AP-Net. Note that polymorph ranking must also account for monomer strain, zero-point vibrational energy, and finite temperature and pressure.[54]

We performed a preliminary experiment to assess AP-Net at ranking polymorphs of the 5-fluorouracil crystal. 61 low-lying 5-fluorouracil crystal structures, one of which is the experimentally observed form II, were taken from the work of Price.[55] The CrystaLattE program[53] was used to reduce each crystal structure into a set of unique dimers, from which the crystal lattice energies were computed at the SAPT0/aDZ level of theory and predicted with AP-Net. An intermolecular closest contact cutoff of 15 Å was used to generate the dimers. The computed and predicted crystal lattice energies are compared in Fig. 7. Importantly, AP-Net reproduces the approximate ranking of the

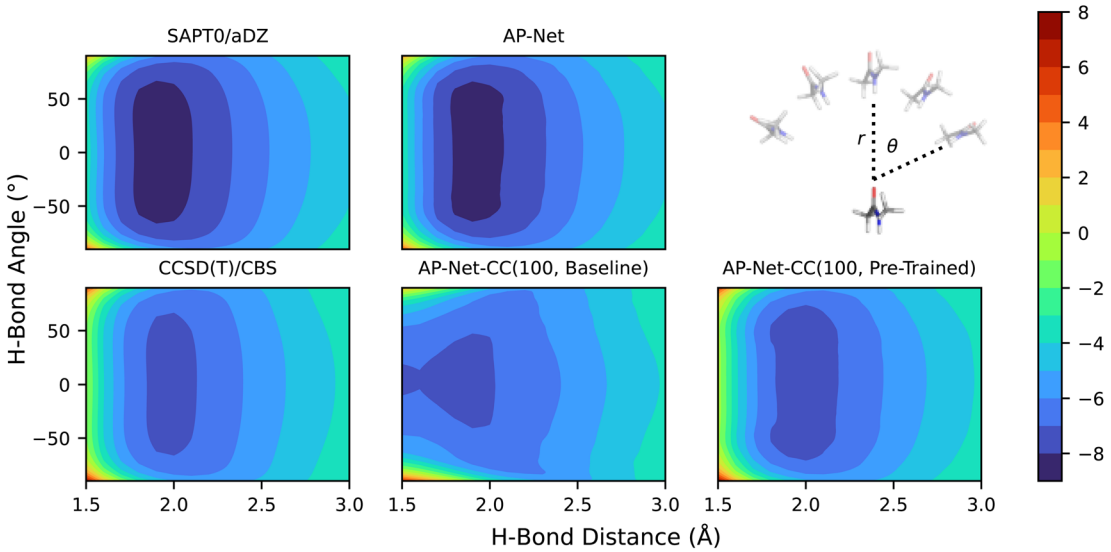

Fig. 6 (Top Right) Visualization of a two-dimensional interaction energy scan (kcal mol^{-1}) for the NMA dimer, varying the hydrogen bond distance (r) and angle (θ). (Top Left) The NMA dimer interaction energy surface computed at the cheaper SAPT0/aDZ level of theory. (Bottom Left) The NMA dimer interaction energy surface computed at the expensive CCSD(T)/CBS level of theory. (Top Center) The NMA dimer interaction energy surface predicted by an AP-Net model trained on ~1.7 million SAPT0/aDZ data points. (Bottom Center) The NMA dimer interaction energy surface predicted by an AP-Net model trained on one hundred CCSD(T)/CBS data points. (Bottom Right) The NMA dimer interaction energy surface predicted by an AP-Net model trained on ~1.7 million SAPT0/aDZ data points and then re-trained with one hundred CCSD(T)/CBS data points. All energies in kcal mol^{-1}.

polymorphs. Form II is correctly predicted to be among the lowest energy structures. The AP-Net ranking of form II happens to be slightly better than that of SAPT0/aDZ due to fortuitous errors in the interaction energies. The MAE of the AP-Net predicted crystal lattice energies relative to SAPT0 is 1.18 kJ mol^{-1}, which is smaller than the disagreement between many quantum chemistry methods.[56] Note that this result is in spite of the fact that AP-Net was trained specifically on protein–ligand data, not 5-fluorouracil homodimers or even ligand–ligand dimers.

The 61 AP-Net crystal lattice energy predictions required less than two CPU minutes, a nearly 30 000-fold savings over the corresponding SAPT0/aDZ cost of 980 CPU hours. Because the cost of quantum chemistry computations scales poorly with system size, AP-Net predicted crystal lattice energies of a larger drug-like molecule would result in even more pronounced savings relative to SAPT0/aDZ.

3 Materials and methods

3.1 Implementation

The AP-Net model was implemented using version 2.3 of the TensorFlow Python package.[57] The implementation and architectural details of the two constituent modules of the AP-Net model are described below.

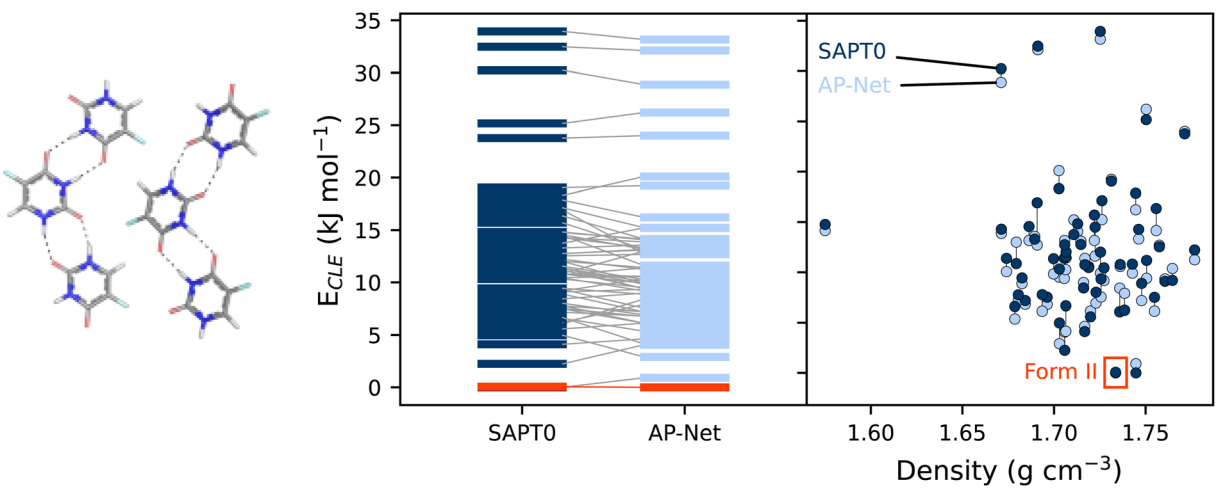

Fig. 7 (Left) The experimentally observed form II of the 5-fluorouracil crystal. (Center) Comparison between computed and predicted relative crystal lattice energies. (Right) Relative crystal lattice energies as a function of density.

3.1.1 Atomic property module. The atomic property module predicts charges, dipoles, and Cartesian quadrupoles of all atoms in a molecule from the identities and coordinates of the atoms and the total charge of the molecule *via* an equivariant MPNN. Reference and predicted multipoles are written as (q, μ, θ) and $(\hat{q}, \hat{\mu}, \hat{\theta})$ respectively.

The initial environment of atom i in the MPNN is a simple mapping or embedding of the integer nuclear charge (Z_i) to a vector $(\boldsymbol{h}_i^0)$ as was proposed in SchNet.[22] The mappings are generated at uniform random for all Z corresponding to atomic elements of interest: H, C, N, O, F, Na, P, S, Cl, and Br. An edge between atoms i and j exists if the distance between the atoms is less than a cutoff distance, r_c, which is set to 5.0 Å. The edge feature vector $\boldsymbol{e}_{ij}$, is a simple encoding of the scalar distance $|\boldsymbol{r}_{ij}|$ using a set of Bessel functions as described in the work of Gasteiger, *et al.*:[32]

$$\boldsymbol{e}_{ij} = [e_{ij,1},\ldots,e_{ij,N}], \tag{1}$$

$$e_{ij,n} = \sqrt{\frac{2}{r_c}}\,\frac{\sin\left(\frac{n\pi}{r_c}|\boldsymbol{r}_{ij}|\right)}{|\boldsymbol{r}_{ij}|}. \tag{2}$$

The message sent from atom i to atom j at time step $t \geq 0$ is an outer product between concatenated hidden state vectors and the edge vector:

$$\boldsymbol{m}_{ij}{}^t = (\boldsymbol{h}_i^0, \boldsymbol{h}_i{}^t, \boldsymbol{h}_j^0, \boldsymbol{h}_j{}^t) \times (1, \boldsymbol{e}_{ij}). \tag{3}$$

The total, directionless message received by atom i at time-step t is a sum over individual messages from all neighbors j:

$$\boldsymbol{m}_i{}^t = \sum_{j \in \mathcal{N}(i)} \boldsymbol{m}_{ij}{}^t, \tag{4}$$

and this quantity is used to update the total, directionless hidden state of atom i:

$$\boldsymbol{h}_i{}^{t+1} = U^t(\boldsymbol{m}_i{}^t), \tag{5}$$

where U^t is a dense, feed-forward neural network. The predicted charge of atom i, $\hat{q}_i$ is determined from the hidden states through all T time steps and a set of dense, feed-forward neural networks:

$$\hat{q}_i = \sum_{0 \leq t \leq T} R^t(\boldsymbol{h}_i{}^t). \tag{6}$$

We set $T = 3$ in this work.

The displacement vector and displacement unit vector between atoms i and j are simply:

$$\boldsymbol{r}_{ij} = \boldsymbol{r}_j - \boldsymbol{r}_i, \tag{7}$$

$$\hat{\boldsymbol{r}}_{ij} = \frac{\boldsymbol{r}_{ij}}{|\boldsymbol{r}_{ij}|}. \tag{8}$$

A directional hidden state, $\boldsymbol{x}_i^t$, for predicting atomic dipoles is determined, analogous to charges:

$$\boldsymbol{x}_i{}^t = \sum_{j \in \mathcal{N}(i)} \hat{\boldsymbol{r}}_{ij} \times D^t\left(\boldsymbol{m}_{ij}{}^t\right), \tag{9}$$

using a directional update function, D. Note that D itself has no directional properties as it operates on the rotational invariant $(\boldsymbol{m}_{ij})$. The functional is named so because it is used to predict a directional hidden state, $\boldsymbol{x}_i^t$ which differs from $\boldsymbol{h}_i{}^t$ in that is has an additional Cartesian dimension. The Cartesian dimension of the directional hidden state inherits the rotational equivariance of the displacement vector $\hat{\boldsymbol{r}}_{\mathrm{ij}}$, which is then used to predict a rotationally equivariant dipole vector:

$$\hat{\mu}_i = \sum_{1 \leq t \leq T} R_\mu{}^t(\boldsymbol{x}_{i,\mu}{}^t). \tag{10}$$

The dipole readout function $R_\mu{}^t$ is made to be a simple linear layer. This ensures rotationally equivariant atomic dipoles; a readout function with non-linearites, such as a dense feed-forward neural network, would not preserve the equivariance of the hidden state vector $\boldsymbol{x}_i{}^t$. Also, the dipole hidden state at $t = 0$ isn't incorporated into the readout because a non-interacting atom has no dipole. Quadrupoles are predicted analogously to dipoles, with separate quadrupole hidden states, update functions, and readout functions.

Lastly, the network architecture enforces conservation of total molecular charge, Q:

$$\hat{q}_i \leftarrow \hat{q}_i + \frac{Q - \sum_i \hat{q}_i}{N}, \tag{11}$$

and also that the Cartesian quadrupoles are symmetric and traceless:

$$\widehat{\Theta} \leftarrow \frac{1}{2}\left(\widehat{\Theta} + \widehat{\Theta}^\dagger\right), \tag{12}$$

$$\widehat{\Theta} \leftarrow \widehat{\Theta} - \frac{\widehat{\Theta}_{xx} + \widehat{\Theta}_{yy} + \widehat{\Theta}_{zz}}{3}\mathscr{I}. \tag{13}$$

3.1.2 Interaction energy module. The interaction energy module predicts the SAPT decomposition of the interaction energy (electrostatics, exchange, induction, and dispersion) from a molecular dimer, which consists of two sets of atomic identities and coordinates and two molecular charges. The characters a, a', b, and b' will be used to index atoms in monomers $\mathscr{A}$ and $\mathscr{B}$, respectively. The interaction energy components are predicted through learned, intermolecular, atomic-pairwise partition:

$$\Delta E_{\mathrm{int}} = \begin{bmatrix} E_{\mathrm{elst}} \\ E_{\mathrm{exch}} \\ E_{\mathrm{ind}} \\ E_{\mathrm{disp}} \end{bmatrix} = \sum_{a \in \mathscr{A}} \sum_{b \in \mathscr{B}} \begin{bmatrix} E_{ab,\mathrm{elst}} \\ E_{ab,\mathrm{exch}} \\ E_{ab,\mathrm{ind}} \\ E_{ab,\mathrm{disp}} \end{bmatrix}. \tag{14}$$

The interaction energy module uses an MPNN architecture similar to that of the atomic property module. Specifically, the message and update functions in this module are identical, but have different weights.

$$\boldsymbol{m}_{aa'}{}^t = \left(\boldsymbol{h}_a{}^0, \boldsymbol{h}_a{}^t, \boldsymbol{h}_{a'}{}^0, \boldsymbol{h}_{a'}{}^t\right) \times \left(1, \boldsymbol{e}_{aa'}\right), \tag{15}$$

$$\boldsymbol{m}_a{}^t = \sum_{a' \in \mathcal{N}(a)} \boldsymbol{m}_{aa'}{}^t, \tag{16}$$

$$\boldsymbol{h}_a{}^{t+1} = U^t(\boldsymbol{m}_a{}^t). \tag{17}$$

In addition to the rotational invariant hidden state vector ($\boldsymbol{h} \in \mathscr{R}^f$), a directional, rotationally equivariant hidden state vector ($\boldsymbol{x} \in \mathscr{R}^{3f}$) is also updated throughout the message passing:

$$\boldsymbol{x}_a{}^{t+1} = \sum_{a' \in \mathcal{N}(a)} \hat{\boldsymbol{r}}_{aa'} \times D^t\left(\boldsymbol{m}_{aa'}{}^t\right), \tag{18}$$

using another feed-forward neural network, D^t. The hidden states from each iteration are concatenated, and a pair feature vector is then created from all hidden state vectors for each intermolecular (a, b) pair:

$$\boldsymbol{h}_a = (\boldsymbol{h}_a^0, \ldots, \boldsymbol{h}_a{}^T), \tag{19}$$

$$\boldsymbol{x}_a = (\boldsymbol{x}_a^0, \ldots, \boldsymbol{x}_a^T), \tag{20}$$

$$\boldsymbol{p}_{ab} = (\hat{q}_a, \hat{q}_b, \boldsymbol{h}_a, \boldsymbol{h}_b, \hat{\boldsymbol{r}}_{ab} \cdot \boldsymbol{x}_a, \hat{\boldsymbol{r}}_{ba} \cdot \boldsymbol{x}_b). \tag{21}$$

Note that this pair feature vector uses the predicted atomic charges from the atomic property module, which is separately applied to both monomers in the dimer. Also, the rotationally equivariant vectors $\boldsymbol{x}$ are incorporated in a rotationally invariant way by projection onto the intermolecular unit vector. Four dense feed-forward NNs are used to predict the four SAPT components from the pair feature vectors:

$$E_{ab,\mathrm{comp}} = |\boldsymbol{r}_{ab}|^{-p}[R^{\mathrm{comp}}(\boldsymbol{p}_{ab}) + R^{\mathrm{comp}}(\boldsymbol{p}_{ba})], \tag{22}$$

where comp is one of the four SAPT components (electrostatics, exchange, induction, dispersion). The pair energies are inversely scaled by the interatomic distance raised to the p power, where p is fixed at 3 across all interaction types; the key consideration was to enforce asymptotic decay of the interaction energy. The output is also symmetrized over the order of the two atoms. Finally, in the case of electrostatic energies, the neural network predictions are corrections on top of multipolar (mtp) electrostatics computed from the charges, dipoles, and quadrupoles predicted by the atomic property module:

$$E_{ab,\mathrm{elst}} \leftarrow E_{ab,\mathrm{elst}} + E_{ab,\mathrm{mtp}}. \tag{23}$$

The predicted interaction energy, though defined as a sum of atom-pair interaction energies, is still a many-body quantity (where "body" refers to atoms). This is a consequence of using a MPNN to featurize each atom with its local atomic environment. In contrast, AP-Net produces a strictly two-body dimer interaction energy (where "body" refers to molecules).

3.2 Training data and procedure

The AP-Net model is trained in a two step procedure. All code used to train this model is present in the AP-Net GitHub repository.[58] First, the atomic property module is trained on a dataset of molecular monomers and computed atomic multipoles. This was done with our previous dataset of 46 623 mostly drug-like fragments and corresponding atomic multipoles computed from HF/cc-pVDZ wavefunctions and partitioned with the minimal basis iterative stockholder (MBIS) scheme.[59] Because the dataset lacks non-neutral monomers and monomers representing protein systems, it was further expanded to include monomers present in the Splinter dataset. 6550 additional computations were performed on randomly selected monomers from the Splinter dataset, totaling 53 173 monomers. The 53 173 monomers were then randomly split into training and validation subsets of 47 855 and 5318 monomers.

The atomic property module was constructed with three message passing iterations. Each dense feed-forward neural network in the module is composed of three hidden layers with 256, 128, and 64 neurons. The ReLU activation function is applied after each hidden layer, followed by an appropriately sized linear operation after the last hidden layer. The edge feature vectors are constructed from 8 Bessel functions and a radial cutoff of 5 Å. Training was performed to minimize the sum of the mean squared errors of the atomic charges, dipoles, and quadrupoles:

$$\mathscr{L} = \frac{1}{N_a}\sum_{a}^{N_a}(q_a - \hat{q}_a)^2 + |\mu_a - \hat{\mu}_a|^2 + \left|\theta_a - \hat{\theta}_a\right|^2 \tag{24}$$

where a indexes atoms in a batch of molecules. The atomic property module was trained for 500 epochs with a batch size of 16 molecules. Weights were optimized with the Adam optimizer using a learning rate of 5×10^{-4}. The weights of the epoch with the lowest validation MSE are used in the final AP-Net model.

In the second step of training, the interaction energy module is trained on the Splinter dimer dataset to predict SAPT decomposed interaction energies. The interaction energy module requires atomic multipoles as an input, which were obtained from the atomic property module. The architecture of the MPNN in this module is identical to that of the atomic property module. Intermolecular atom pair readouts are performed with an 8 Å cutoff. This means that the interaction energy of atom pairs within this cutoff is predicted with a full neural network inference; the interaction energy of atom pairs outside of this cutoff is only accounted for by multipolar electrostatics. The asymptotic decay coefficient (p) was set to three. Random training and validation subsets of 1.5M and 150K dimers are taken from the 1.66M dimers in the Splinter dataset. The module is optimized to minimize the MSE of the individual SAPT components:

$$\mathscr{L} = \frac{1}{N_d}\sum_{d}^{N_d}\sum_{c}^{4}\left(E_{c,d} - \hat{E}_{c,d}\right)^2, \tag{25}$$

where c is one of four SAPT components (electrostatics, exchange, induction, and dispersion) and d indexes dimers in the batch. The MPNN was trained using a batch size of 16 dimers and the Adam optimizer with a learning rate of 5×10^{-4}. Training was performed for 50 epochs, and the weights of the epoch with the lowest validation MSE are used in the final AP-

Net model. An ensemble of five randomly initialized AP-Net models were trained on the same data to reduce uncertainty, and all predictions presented in this work are the average prediction of the ensemble.

3.3 SAPT-PDB-13K dataset preparation

The SAPT-PDB-13K test set of 13 216 dimers was prepared to consist of diverse, drug-like molecules paired with mono- and dipeptides extracted from crystallographic structures deposited in the PDB. The following procedure was followed to ensure that ligands were structurally diverse and drug-like: ligand molecules were extracted from the PDBbind 2019 refined set of 4852 complexes,[60,61] imported into Maestro 2021-3,[62] assigned charges and bond orders with LigPrep[63] and clustered using the spectral clustering utility with default settings, which provided 133 representative ligands. An additional 600 ligands were visually selected which further added structural diversity and represented the full range of elements compatible with the AP-Net model (H, C, N, O, F, Na, P, S, Cl, and Br). The corresponding 733 PDB protein/ligand complexes were subjected to refinement using the Schrodinger Protein Prep[64] tool with default settings. Dimers consisting of ligands and proximal mono- and dipeptides were created, wherein the N- and C-termini were capped with acetyl and N–Me groups, respectively. Visual inspection led to removal of erroneous structures (*e.g.*, presence of hypervalent carbons or otherwise non-physical geometries) and duplicates. SAPT0/aug-cc-pV(D+d)Z interaction energies of the 13 216 dimers were computed with Psi4 and made available in the ESI.†

4 Discussion

The AP-Net potential developed in this work is a robust, physically-motivated NN intermolecular interaction model. In contrast to the many general purpose ML potentials which predict a total energy, the AP-Net potential predicts interaction energies. As a consequence of this specialization, AP-Net is constructed to adhere to known physical priors of intermolecular interactions, such as their approximate atomic pairwise nature and distance decay. An additional physical prior is captured by AP-Net's unique two-component architecture. Rather than simply predict atom-pair contributions to the interaction energy, AP-Net is constructed to predict monomer electron densities (in the form of atom-centered multipoles), evaluate a long-range electrostatic interaction energy from the predicted multipoles, and then predict atom-pair corrections to this evaluated energy.

This two-component architecture confers a number of advantages to the AP-Net model. Because of the multipolar electrostatic force field, the AP-Net model produces electrostatic interaction energies that are asymptotically exact at the target level of theory using a relatively small amount of multipole training data. An analogous pure-NN model would need to be trained on an intractable number of dimer interaction energies to reach the same level of accuracy. This case of long-range electrostatics illustrates a weakness of NN models, which is that unnecessary flexibility can be a detriment to data efficiency. AP-Net's architecture effectively limits the flexibility of the functional form at long-range where the physics is known, allowing the modeling capacity to be applied to the more difficult short-range interactions. In addition to improving the data efficiency of the model, concentrating on short-range intermolecular interactions improves the computational efficiency of the AP-Net model. Neural network inferences, which are more expensive than force field evaluations, are only required for pairs of interaction atoms within a relatively short distance threshold (8 Å).

This physically-motivated AP-Net is applied to the challenging and consequential problem of modeling protein–ligand interaction energies. A useful AP-Net model is made possible by the Splinter dataset: a comprehensive and diverse collection of 1.66M protein–ligand dimers and SAPT0 interaction energies. The trained AP-Net accurately reproduces the SAPT decomposition of interaction energies well within chemical accuracy in the great majority of cases. More importantly, generalizability to larger models of protein–ligand dimers is observed, with good agreement between AP-Net and SAPT0 for substituent effects for ~200-atom model systems where SAPT0 results can still be obtained. While the SAPT0 computations require many hours, the AP-Net results run in seconds. These findings suggest that the AP-Net model is an immediately practical tool for drug design research when quantum-level accuracy is desired for protein–ligand interaction energies, as was helpful in previous studies by our group on factor Xa inhibitors.[11]

This AP-Net model is not without shortcomings. One apparent deficiency is the underestimation of strong induction interactions, which occurs for a few select realistic protein–ligand dimers of the SAPT-PDB-13K dataset. These dimers represent an edge case where the non-local, many-body nature is poorly captured by the atomic-pairwise architecture of AP-Net. Efficiently modeling this non-pairwise additivity likely requires a model architecture with an appropriate inductive bias. In the same way that the current AP-Net model fuses classical long-range multipole electrostatics with a NN-predicted short-range correction, a future AP-Net model might benefit from incorporating a classical Thole-type induction model as is done in polarizable *ab initio* force fields like AMOEBA.[65,66] This could be incorporated by training the atomic property module to predict atomic polarizability tensors. Another potential limitation arises from using a framework of interacting monomers to predict intermolecular interaction energies. This framework is largely incompatible with reactive chemistry, where the formation or dissolution of bonds changes the definition of monomers. Modeling reactive chemistry with an intermolecular potential can be done with the empirical valence bond (EVB) approach,[25,67] but it might be easier to simply train a NN potential to the total system energy.

Because of the high accuracy of AP-Net relative to SAPT0, the development of future models will likely target training data computed at a higher level of quantum chemistry theory. Additional AP-Net model development, whether targeting new levels of theory or new types of dimers, can benefit from transfer learning from the current, general, protein–ligand model. This

approach greatly reduces training data requirements. Surprisingly, the protein–ligand AP-Net model can be used for modeling ligand–ligand interaction energies accurately enough to rank polymorphs of the 5-fluorouracil crystal, an application far outside of the original intention of the AP-Net model. This result illustrates one of many potential future AP-Net use cases, and it also points towards the possibility of a universal interaction energy potential.

Data availability

The AP-Net model has been trained on the Splinter Dataset (ref. 42). The remaining data supporting this article have been included as part of the ESI.† The code for AP-Net can be found at **https://github.com/zachglick/apnet** with DOI **https://doi.org/10.5281/zenodo.11493604**. The version of the code employed for this study is version 0.1.1.

Author contributions

Conceptualization: ZLG, DPM, SAS, AK, DLC, CDS. Methodology: ZLG, DPM, CSG, SAS, AK, CDS. Investigation: ZLG. Visualization: ZLG. Supervision: CDS and DLC. Writing – original draft: ZLG. Writing – review & editing: CDS, DLC, ZLG, DPM.

Conflicts of interest

There are no conflicts to declare.

Acknowledgements

The authors gratefully acknowledge financial support from the Department of Research and Early Development Information Technology, Bristol Myers Squibb, and the U. S. National Science Foundation through a grant to CDS (CHE-1955940) and an NSF Graduate Research Fellowship to CSG (DGE-2039655). Any opinion, findings, and conclusions or recommendations expressed in this material are those of the authors and do not necessarily reflect the views of the National Science Foundation. The authors thank S. Price for for providing computationally predicted 5-fluorouracil crystal structures. The authors also thank Andrea Bortolato for his assistance in constructing the SAPT-PDB-13K test set.

Notes and references

1 L. Strekowski and B. Wilson, *Mutat. Res.*, 2007, **623**, 3–13.
2 A. Bodley, L. F. Liu, M. Israel, R. Seshadri, Y. Koseki, F. C. Giuliani, S. Kirschenbaum, R. Silber and M. Potmesil, *Cancer Res.*, 1989, **49**, 5969–5978.
3 H. J. Davis and R. J. Phipps, *Chem. Sci.*, 2017, **8**, 864–877.
4 B. Huang, S. Muy, S. Feng, Y. Katayama, Y.-C. Lu, G. Chen and Y. Shao-Horn, *Phys. Chem. Chem. Phys.*, 2018, **20**, 15680–15686.
5 B. Rybtchinski, *ACS Nano*, 2011, **5**, 6791–6818.
6 B. Jeziorski, R. Moszynski and K. Szalewicz, *Chem. Rev.*, 1994, **94**, 1887–1930.
7 K. Szalewicz, *Wiley Interdiscip. Rev.: Comput. Mol. Sci.*, 2011, **2**, 254–272.
8 K. Patkowski, *Wiley Interdiscip. Rev.: Comput. Mol. Sci.*, 2020, **10**, e1452.
9 C. D. Sherrill, *Acc. Chem. Res.*, 2012, **46**, 1020–1028.
10 R. M. Parrish, T. M. Parker and C. D. Sherrill, *J. Chem. Theory Comput.*, 2014, **10**, 4417–4431.
11 R. M. Parrish, D. F. Sitkoff, D. L. Cheney and C. D. Sherrill, *Chem.–Eur. J.*, 2017, **23**, 7887–7890.
12 J. Behler and M. Parrinello, *Phys. Rev. Lett.*, 2007, **98**, 146401.
13 C. M. Handley and P. L. A. Popelier, *J. Phys. Chem. A*, 2010, **114**, 3371–3383.
14 J. Behler, *Chem. Rev.*, 2021, **121**, 10037–10072.
15 O. T. Unke, S. Chmiela, M. Gastegger, K. T. Schütt, H. E. Sauceda and K.-R. Müller, *Nat. Commun.*, 2021, **12**, 7273.
16 J. Wang, S. Olsson, C. Wehmeyer, A. Pérez, N. E. Charron, G. De Fabritiis, F. Noé and C. Clementi, *ACS Cent. Sci.*, 2019, **5**, 755–767.
17 R. Ramakrishnan, P. O. Dral, M. Rupp and O. A. v. Lilienfeld, *Sci. Data*, 2014, **1**, 140022.
18 S. Chmiela, A. Tkatchenko, H. E. Sauceda, I. Poltavsky, K. T. Schütt and K.-R. Müller, *Sci. Adv.*, 2017, **3**, e1603015.
19 J. S. Smith, R. Zubatyuk, B. Nebgen, N. Lubbers, K. Barros, A. E. Roitberg, O. Isayev and S. Tretiak, *Sci. Data*, 2020, **7**, 134.
20 A. G. Donchev, A. G. Taube, E. Decolvenaere, C. Hargus, R. T. McGibbon, K.-H. Law, B. A. Gregersen, J.-L. Li, K. Palmo, K. Siva, M. Bergdorf, J. L. Klepeis and D. E. Shaw, *Sci. Data*, 2021, **8**, 55.
21 J. S. Smith, O. Isayev and A. E. Roitberg, *Chem. Sci.*, 2017, **8**, 3192–3203.
22 K. T. Schütt, H. E. Sauceda, P.-J. Kindermans, A. Tkatchenko and K.-R. Müller, *J. Chem. Phys.*, 2018, **148**, 241722.
23 K. Yao, J. E. Herr, D. Toth, R. Mckintyre and J. Parkhill, *Chem. Sci.*, 2018, **9**, 2261–2269.
24 D. A. Rufa, H. E. B. Macdonald, J. Fass, M. Wieder, P. B. Grinaway, A. E. Roitberg, O. Isayev and J. D. Chodera, *bioRxiv*, 2020, DOI: **10.1101/2020.07.29.227959**.
25 J. P. Stoppelman and J. G. McDaniel, *J. Chem. Phys.*, 2021, **155**, 104112.
26 J. Gilmer, S. S. Schoenholz, P. F. Riley, O. Vinyals and G. E. Dahl, *Proceedings of the 34th International Conference on Machine Learning*, Sydney, NSW, Australia, 2017, pp. 1263–1272.
27 V. G. Satorras, E. Hoogeboom and M. Welling, *Proceedings of the 38th International Conference on Machine Learning*, 2021, pp. 9323–9332.
28 T. E. Smidt, *Trends Chem.*, 2021, **3**, 82–85.
29 M. Geiger and T. Smidt, *arXiv*, preprint, arXiv:2207.09453, 2022, DOI: **10.48550/arxiv.2207.09453**.
30 S. Batzner, A. Musaelian, L. Sun, M. Geiger, J. P. Mailoa, M. Kornbluth, N. Molinari, T. E. Smidt and B. Kozinsky, *Nat. Commun.*, 2022, **13**, 2453.

31 I. Batatia, D. P. Kovacs, G. Simm, C. Ortner and G. Csanyi, *Adv. Neural Inf. Process. Syst.*, 2022, 11423–11436.
32 J. Gasteiger, J. Groaa and S. Günnemann, *International Conference on Learning Representations*, 2020.
33 S. Takamoto, S. Izumi and J. Li, *Comput. Mater. Sci.*, 2022, **207**, 111280.
34 Z. L. Glick, D. P. Metcalf, A. Koutsoukas, S. A. Spronk, D. L. Cheney and C. D. Sherrill, *J. Chem. Phys.*, 2020, **153**, 044112.
35 D. Rosenberger, J. S. Smith and A. E. Garcia, *J. Phys. Chem. B*, 2021, **125**, 3598–3612.
36 K. K. Huguenin-Dumittan, P. Loche, N. Haoran and M. Ceriotti, *J. Phys. Chem. Lett.*, 2023, **14**, 9612–9618.
37 M. Konrad and W. Wenzel, *J. Chem. Theory Comput.*, 2021, **17**, 4996–5006.
38 I.-B. Magdău, D. J. Arismendi-Arrieta, H. E. Smith, C. P. Grey, K. Hermansson and G. Csányi, *npj Comput. Mater.*, 2023, **9**, 146.
39 Z. L. Glick, A. Koutsoukas, D. L. Cheney and C. D. Sherrill, *J. Chem. Phys.*, 2021, **154**, 224103.
40 D. P. Metcalf, A. Jiang, S. A. Spronk, D. L. Cheney and C. D. Sherrill, *J. Chem. Inf. Model.*, 2021, **61**, 115–122.
41 R. Ramakrishnan, P. O. Dral, M. Rupp and O. A. v. Lilienfeld, *J. Chem. Theory Comput.*, 2015, **11**, 2087–2096.
42 S. A. Spronk, Z. L. Glick, D. P. Metcalf, C. D. Sherrill and D. L. Cheney, *Sci. Data*, 2023, **10**, 619.
43 T. M. Parker, L. A. Burns, R. M. Parrish, A. G. Ryno and C. D. Sherrill, *J. Chem. Phys.*, 2014, **140**, 094106.
44 T. Helgaker, T. A. Ruden, P. Jørgensen, J. Olsen and W. Klopper, *J. Phys. Org. Chem.*, 2004, **17**, 913–933.
45 D. P. Metcalf, A. Koutsoukas, S. A. Spronk, B. L. Claus, D. A. Loughney, S. R. Johnson, D. L. Cheney and C. D. Sherrill, *J. Chem. Phys.*, 2020, **152**, 074103.
46 A. Stone, *The Theory of Intermolecular Forces*, Oxford University Press, 2013.
47 J. B. Schriber, D. R. Nascimento, A. Koutsoukas, S. A. Spronk, D. L. Cheney and C. D. Sherrill, *J. Chem. Phys.*, 2021, **154**, 184110.
48 K. Raghavachari, G. W. Trucks, J. A. Pople and M. Head-Gordon, *Chem. Phys. Lett.*, 1989, **157**, 479–483.
49 K. Weiss, T. M. Khoshgoftaar and D. Wang, *J. Big Data*, 2016, **3**, 9.
50 J. S. Smith, B. T. Nebgen, R. Zubatyuk, N. Lubbers, C. Devereux, K. Barros, S. Tretiak, O. Isayev and A. E. Roitberg, *Nat. Commun.*, 2019, **10**, 2903.
51 G. P. Stahly, *Cryst. Growth Des.*, 2007, **7**, 1007–1026.
52 A. M. Reilly, R. I. Cooper, C. S. Adjiman, S. Bhattacharya, A. D. Boese, J. G. Brandenburg, P. J. Bygrave, R. Bylsma, J. E. Campbell, R. Car, *et al.*, *Acta Crystallogr., Sect. B*, 2016, **72**, 439–459.
53 C. H. Borca, B. W. Bakr, L. A. Burns and C. D. Sherrill, *J. Chem. Phys.*, 2019, **151**, 144103.
54 G. J. O. Beran, *Chem. Rev.*, 2016, **116**, 5567–5613.
55 A. T. Hulme, S. L. Price and D. A. Tocher, *J. Am. Chem. Soc.*, 2005, **127**, 1116–1117.
56 J. Brandenburg and S. Grimme, *Acta Crystallogr., Sect. B*, 2016, **72**, 502–513.
57 M. Abadi, A. Agarwal, P. Barham, E. Brevdo, Z. Chen, C. Citro, G. S. Corrado, A. Davis, J. Dean, M. Devin, S. Ghemawat, I. Goodfellow, A. Harp, G. Irving, M. Isard, Y. Jia, R. Jozefowicz, L. Kaiser, M. Kudlur, J. Levenberg, D. Mane, R. Monga, S. Moore, D. Murray, C. Olah, M. Schuster, J. Shlens, B. Steiner, I. Sutskever, K. Talwar, P. Tucker, V. Vanhoucke, V. Vasudevan, F. Viegas, O. Vinyals, P. Warden, M. Wattenberg, M. Wicke, Y. Yu and X. Zheng, *TensorFlow: Large-Scale Machine Learning on Heterogeneous Distributed Systems*, 2016.
58 Z. L. Glick, *zachglick/apnet: v0.1.1*, 2022, DOI: **10.5281/zenodo.11493604**.
59 T. Verstraelen, S. Vandenbrande, F. Heidar-Zadeh, L. Vanduyfhuys, V. V. Speybroeck, M. Waroquier and P. W. Ayers, *J. Chem. Theory Comput.*, 2016, **12**, 3894–3912.
60 Z. Liu, M. Su, L. Han, J. Liu, Q. Yang, Y. Li and R. Wang, *Acc. Chem. Res.*, 2017, **50**, 302–309.
61 Y. Li, Z. Liu, J. Li, L. Han, J. Liu, Z. Zhao and R. Wang, *J. Chem. Inf. Model.*, 2014, **54**, 1700–1716.
62 *Schrödinger Release 2021-1*, Maestro, Schrödinger, LLC, New York, NY, 2021.
63 *Schrödinger Release 2021-1*, LigPrep, Schrödinger, LLC, New York, NY, 2021.
64 *Schrödinger Release 2021-1: Protein Preparation Wizard*, Epik, Schrödinger, LLC, New York, NY, 2021; Impact, Schrödinger, LLC, New York, NY; Prime, Schrödinger, LLC, New York, NY, 2021.
65 B. T. Thole, *Chem. Phys.*, 1981, **59**, 341–350.
66 J. W. Ponder, C. Wu, P. Ren, V. S. Pande, J. D. Chodera, M. J. Schnieders, I. Haque, D. L. Mobley, D. S. Lambrecht, R. A. DiStasio Jr, *et al.*, *J. Phys. Chem. B*, 2010, **114**, 2549–2564.
67 S. C. Kamerlin and A. Warshel, *Wiley Interdiscip. Rev.: Comput. Mol. Sci.*, 2011, **1**, 30–45.